2021 43rd Annual International Conference of the
IEEE Engineering in Medicine & Biology Society (EMBC)
Oct 31 - Nov 4, 2021. Virtual Conference

Geometric Generalization of Self Tapping Screw Insertion Model

Jack Wilkie[1], Paul D. Docherty[1,2], Thomas Stieglitz[3], and Knut Möller[1]

***Abstract*— Bone screws are used in orthopaedic procedures to fix implants and stabilise fractures. These procedures require care, as improperly torquing the screws can lead to implant failure or tissue damage, potentially requiring revision surgery or causing further disability. It was proposed that automated torque-limit identification may allow clinical decision support to control the screw torque, and lead to improved patient outcomes. This work extends a previous model of the screw insertion process to model complex thread geometries used for bone screws; consideration was made for the variable material properties and behaviours of bone to allow further tuning in the future. The new model was simulated and compared with the original model. The model was found to be in rough agreement with the earlier model, but was distinct, and could model thread features that the earlier model could not, such as the fillets and curves on the bone screw profile. The new model shows promise in modelling the more advanced thread geometries of bone screws with higher accuracy.**

***Clinical relevance:* This work extends a self tapping screw model to support complex thread shapes, as common in bone screws, allowing more accurate modelling of the clinically relevant geometries.**

I. Introduction

Bone screws are used in many orthopaedic procedures, primarily to fix implants in bone, or for stabilising fractured bone to facilitate natural healing. Incorrect torquing of bone screws through under- or over-tightening can result in screw loosening [1] or thread stripping [2], which may cause implant failure and/or tissue damage [3]; these can be costly and risky to remedy with revision surgery.

Surgeons currently torque screws in an *ad-hoc* manner. While experienced surgeons can achieve good results, the potential for error remains [4]. Wilkie *et al.* [5] proposed that an automated system for bone screw torque limitation could provide more intelligent control over bone screw torquing, leading to better patient outcomes. This system could operate by monitoring signals from the screwing process such as torque and angular displacement over time. These signals would be used to fit a model of the screwing process. The model would have unknown parameters for the bone material properties, hence fitting the model in a real-time clinical setting would determine these patient-specific properties. The bone properties could then be combined with known information about the screw, hole, and implant geometry to estimate the optimal torque for the screw. This optimal torque could then be used through a torque indicator or limiter to allow optimal screw torquing.

Seneviratne *et al.* generated a seminal model of self-tapping screw mechanics. More recently, this was developed further [6] and successfully tested computationally for identifiability [7], and has had some initial experimental validation [8]. Primarily, this paper will focus on expanding the accuracy of modelling bone screw thread profiles, which are more complex than typical machine screws (Shown in Fig. 1). Secondarily, we will provide a flexible system for representing the friction stress (σ_f), which varies over the surface of the screw thread, expanding upon Seneviratne *et al.* [9], which used a constant σ_f which can be assumed to be approximately equal to the compressive strength of the material.

II. Methods

A. Definitions

A single screw thread profile is modelled as a parametric curve $r(t), z(t)$ where $t \in [t_0, t_f]$, as shown in Fig. 1, where r is the radial distance from the screw centreline, and z is the vertical position along the screw centreline. A helical co-ordinate, ϕ, follows the helix of the screw thread. The position of the thread in r,z co-ordinates generally remains constant as the ϕ co-ordinate changes. D_h is the hole diameter.

Only the part of the thread in contact with the hole is strictly required for this model (as in Fig. 1). However, remaining geometry can also be modelled as it is not inaccurate and will simply be ignored in the torque-rotation model; the full thread may be useful for programmatically analysing varying hole diameters without changing the parametric curve.

B. Friction Component

When a self-tapping screw is inserted, the screw threads push against the hole and deform the material. This is

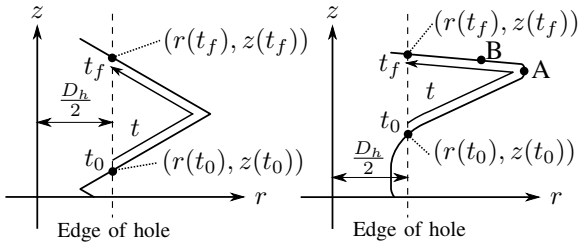

Fig. 1. Example of parametric screw thread representations for a normal screw (Left) and a bone screw approximating ISO 5835:1991's 'deep' thread [10](Right).

*This work was partially supported by grants "CiD" and "Digitalisation in the OR" from BMBF (Project numbers 13FH5E02IA and 13FH5I05IA).

[1]Jack Wilkie, Paul D. Docherty, and Knut Möller are with the Institute for Technical Medicine (ITeM), Hochschule Furtwangen, Jakob-Kienzle-Straße 17, Villingen-Schwenningen, Germany wij@hs-furtwangen.de

[2]Paul D. Docherty is also with the Centre for Bioengineering, University of Canterbury, 20 Kirkwood Avenue, Christchurch, New Zealand

[3]Thomas Stieglitz is with the Department of Microsystems Engineering, University of Freiburg, Georges-Köhler-Allee 102, Freiburg, Germany

initially an elastic deformation process, but transitions to plastic deformation after the materials yield stress is exceeded. Once the screw threads have fully deformed the hole, the material still has its elastic deformation component, which presses against the screw threads, causing friction; the friction stress at a point is generally equivalent to the final stress the thread needed to exert on the hole to deform it at that point. Depending on the material, a good approximation for the friction stress is the compressive yield or ultimate strength, which can be further approximated with the yield or ultimate tensile strength (σ_{uts}). While this combined assumption may exacerbate the imprecision of the model, determining σ_{uts} is much simpler in many cases. σ_{uts} will be used for the remainder of this paper, however if the ultimate compressive stress or friction stress is directly available, it should substituted. This first approximation can be represented as shown in (1). The step function, H, results in zero friction for thread areas not in contact with the hole, allowing those parts to be left in the threads parametric representation.

$$\sigma_f(r) = \begin{Bmatrix} 0, & \text{for } r \leq \frac{D_h}{2} \\ \sigma_{\text{uts}} & \text{for } r > \frac{D_h}{2} \end{Bmatrix} = H\left(r - \frac{D_h}{2}\right)\sigma_{\text{uts}} \quad (1)$$

A more representative model could account for areas near the edge of the hole, where only partial elastic deformation occurs, reducing friction stress. Using C_{max} to represent the maximum deflection distance before plastic deformation, this can be modelled as:

$$\begin{aligned}\sigma_f(r) &= \begin{Bmatrix} 0, & \text{for } r \leq \frac{D_h}{2} \\ \left(r - \frac{D_h}{2}\right)\frac{\sigma_{uts}}{C_{\text{max}}}, & \text{for } \frac{D_h}{2} < r \leq \frac{D_h}{2} + C_{\text{max}} \\ \sigma_{\text{uts}} & \text{for } r > \frac{D_h}{2} \end{Bmatrix} \\ &= \max\left(1, H\left(r - \frac{D_h}{2}\right)\left(r - \frac{D_h}{2}\right)\frac{1}{C_{\text{min}}}\right)\sigma_{\text{uts}}\end{aligned} \quad (2)$$

Additionally, the angle of the thread profile element, denoted here as $\beta(t)$ (In (4)), can be considered, as thread profile segments aligned with the z-axis (e.g. 'A' in Fig. 1) are likely to experience a greater stress than segments more aligned with the r-axis (e.g. 'B' in Fig. 1), because they (A) are pushing into the material instead of (B) sliding past it. A simple approximation of the relative stress can be achieved by modulating the onset of friction stress from 0 on r-axis aligned segments, to the normal value on z-axis aligned segments with a cosine function; this will still reach σ_{uts}, but needs more deflection to do so when the thread angle is sharper:

$$\begin{aligned}&\sigma_f(r, \beta(t)) = \\ &\quad \min\left(1, H\left(r - \frac{D_h}{2}\right)\left(r - \frac{D_h}{2}\right)\frac{\cos(\beta)}{C_{\text{max}}}\right)\sigma_{\text{uts}}\end{aligned} \quad (3)$$

$$\beta(t) = \arctan\left(\frac{dr}{dt}(t) \Big/ \frac{dz}{dt}(t)\right) \quad (4)$$

C_{max} was estimated using ANSYS 18.1. The FEM model consisted of a thin disk with a hole in the middle. The top and bottom surfaces of the disk were constrained to only allow planar displacement, forcing plane strain. The outer diameter of the disk(100 mm) was much larger than the central hole (3.2 mm). The outside face was fixed, and the inside of the hole was given a pressure equal to σ_{uts}. The displacement of the inside edge of the hole was used as C_{max}.

By performing a line integral over the friction stress function along the parametric thread curve, then integrating over the thread helix, the friction torque of the screw can be found. Considering the friction force, δF_μ, on an element of the thread, and accounting for the helix angle of the element, $\theta(t) = \arctan\left(\frac{p}{2\pi r(t)}\right)$ (where p is the thread pitch), then integrating over the thread curve C:

$$\delta F_\mu = \mu \delta F_N = \mu \sigma(t) r(t) d\phi ds \quad (5)$$

$$\begin{aligned}\delta\tau &= \int_C \cos(\theta) F_\mu r = \mu\left(\int_C \cos(\theta(t))\sigma(t) r^2(t) ds\right) d\phi \\ &= \mu\left(\int_{t_0}^{t_f} \cos(\theta(t))\sigma(t) r^2(t)\sqrt{\frac{dr}{dt}(t)^2 + \frac{dz}{dt}(t)^2}\, dt\right) d\phi\end{aligned} \quad (6)$$

$\delta\tau$ can also be considered a function of ϕ, as thread geometry can vary, notably at the tip of the screw, which is often tapered at 45°-60°. Therefore the different friction at the tapered end of the screw can be modelled by modifying the parametric thread model with the definitions $\hat{r}(t) = \min(r(t), az(t) + b\phi)$ and $\hat{z}(t) = z(t)$. For a standard taper, a is calculated from the taper angle θ_{taper} with $a = 1/\tan(\theta_{\text{taper}})$, and b can be determined from a and the thread pitch with $b = \frac{ap}{2\pi}$. The thread should be defined such that the profile beings to touch the hole at $\phi = 0$. This model gives effective thread geometries as shown in Fig. 2. To realise this, all instances of $r(t)$ and $z(t)$ in (6) are substituted with $\hat{r}(t)$ and $\hat{z}(t)$ (redefining σ and θ as $\hat{\sigma}$ and $\hat{\theta}$).

To calculate the total friction torque at a specific angular displacement ϕ, $\delta\tau$ is integrated ($\hat{r}$, $\hat{z}$, $\hat{\sigma}$, and $\hat{\theta}$ are functions of t and ϕ). Equation (7) is expected to be solved numerically.

$$\begin{aligned}\tau_f(\phi) &= \int_0^\phi \delta\tau(\phi) \\ &= \mu\int_0^\phi \left(\int_{t_0}^{t_f} \cos(\hat{\theta})\hat{\sigma}\hat{r}^2\sqrt{\frac{d\hat{r}}{dt}^2 + \frac{d\hat{z}}{dt}^2}\, dt\right) d\phi\end{aligned} \quad (7)$$

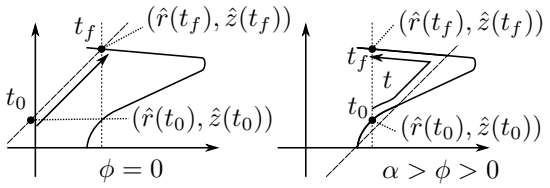

Fig. 2. Effective thread profile considering taper at different angular displacement coordinates. θ_{taper} is defined as the angle between the z axis and the diagonal line.

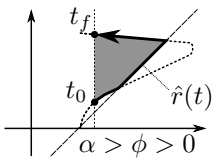

Fig. 3. The stress function multiplied by radius is integrated over the shaded area to get cutting torque.

C. Cutting Component

The other main component of torque is the cutting torque. The cutting section of the screw has to push material out of the way so that it can turn. The stress resisting this cutting will be approximately the same as the σ function described earlier, however here the force is in the helical direction of rotation which directly opposes the turning, so does not depend on μ. This force acts on the cross-sectional area of the thread which is currently engaged in cutting. Hence, the cutting force begins at zero, then increases as the tapered section is inserted, plateaus after this (while ignored here, the torque would ramp down to zero if the screw exited the opposite side of the material). If the screwing direction is reversed, the cutting forces will drop to zero (and the friction on the tapered section will be almost zero).

The cutting torque is calculated by integrating the stress function σ multiplied by r over the currently engaged thread area (Fig. 3). The thread pitch is compensated with $cos(\theta)$ [9]. This is first integrated with dr in a line from $r = \frac{D_h}{2}$ to $r = \max(\hat{r}, \frac{D_h}{2})$, and then integrated over the thread area with $dz = \frac{dz}{dt}(t)dt$ from t_0 to t_f, at angular displacement ϕ:

$$\tau_s(\phi) = \int_{t_0}^{t_f} \left(\int_{\frac{D_h}{2}}^{\hat{r}(t,\phi)} \cos(\theta(r)) r \sigma(r, z(t)) dr \right) \frac{dz}{dt}(t) dt \tag{8}$$

D. Completed Model and Testing

For the model presented here, the total torque as a function of angular displacement is $\tau(\phi) = \tau_f(\phi) + \tau_s(\phi)$.

This model was computationally tested with all three σ functions, and compared to the simpler model from [9]. The models were simulated using a 4.5 mm shallow thread profile (HA 4.5) and a 6.5 mm deep thread profile (HB 6.5) from ISO 5835:1991 [10]. As the thread does not exactly match the parametrised thread in [9], the 2β term was set equal to the total thread thread angle ($\alpha + \beta$ in ISO 5835:1991), and the minor diameter and pitch were used as-is. The hole diameter was 3.2 mm, and the half taper angle is $45°$, which was used to calculate α for the [9] model. Only the friction and cutting components from [9] were used to match the friction and cutting components in the new model. For the material properties, $E = 300$MPa [11], $\sigma_{uts} = 3.5$MPa [11], and $\mu = 0.4$ [12], to represent a normal femoral head, and Poisson's ratio is based on a generic estimate $\nu = 0.3$.

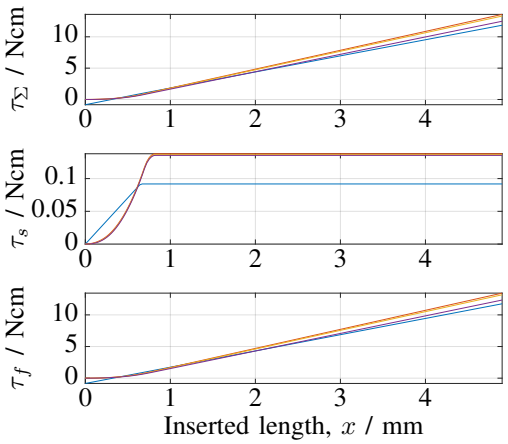

Fig. 4. Total (τ_Σ), cutting (τ_s), and friction (τ_f) torque for HA 4.5 insertion with [9] model in blue, and the proposed model in red (simple σ), yellow (incl. C_{max}), and purple (incl. thread angle). The lines are very close to overlapping.

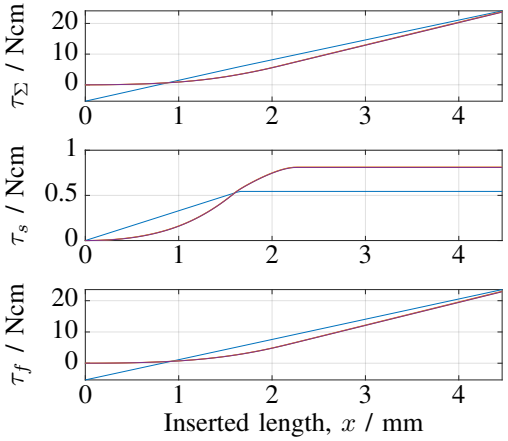

Fig. 5. Total (τ_Σ), cutting (τ_s), and friction (τ_f) torque for HB 6.5 insertion with [9] model in blue, and the proposed model in red (simple σ), yellow (incl. C_{max}), and purple (incl. thread angle). The proposed model lines mostly overlap.

III. Results

The value for C_{max} determined from FEM was 0.0242 mm for the given parameters. The simulated torque-displacement plots for the existing model and proposed models are shown in Fig. 4 and Fig. 5. Note that in Fig. 5 the three new models overlap.

IV. Discussion

The results show that this model gives roughly similar results to [9], which has had experimental validation. This gives confidence that the methodology is sound, and that the derivation lacks serious errors. However, more thorough testing is required to increase the confidence under a wide range of conditions, and to quantify the accuracy.

This model shows notable differences when compared to [9]. The simpler model in [9] produces a plot with straight lines, and simplifies the geometry greatly; the proposed model

is curved in a way that should more accurately represent the interaction between the bone screw thread geometry and the hole. In both cases examined, the new model predicted higher cutting torque forces, which is expected as the thread geometry included extra areas from fillets and other rounding that were neglected in the simpler model [9]. The new model also predicted a higher gradient on the friction forces, which could also be explained with a higher contact area from the curved sections of the thread compared to a strictly triangular profile assumed in [9].

The differences between the σ functions for the new models were also examined. For the HB 6.5 screw, no significant difference can be seen unless examined very closely. However, the HA 4.5 screw showed notable differences for the different model versions, showing that under some circumstances, the differences between the σ function choices can be significant. As each σ function included more considerations, it may be reasonable to assume the more complex ones are more accurate. For shallower profiles like HA 4.5, the total area in contact is relatively low, and the proportion with only slight deformation is relatively high compared to a deep profile like HB 6.5; this means the effects of modelling the lower friction from elastic deformation are more significant, which explains why the models are distinct for HA 4.5 but not HB 6.5. The σ functions could be made arbitrarily complex, and may be used to further improve the model accuracy, accounting for varying material properties and complex material behaviours. For example, changes could be inspired by Finite Element studies into more realistic stress distributions. In particular, these models use a constant σ_{uts} which fails to precisely capture the complex two-way interaction between the screw geometry and hole material like an FE model would. This flexibility may also help with modelling the more complex material properties and structures present in bone.

The C_{max} value has a significant effect on whether the more complex versions of the model are distinct. If low, then there is very little partial deformation to differentiate the different σ functions. The value of C_{max} depends on the hole size and material properties. Using the linearity assumption for the mechanical model, and assuming small deflections, it would be expected that a higher σ_{uts} would require proportionally larger force/deflection before plastic deformation, increasing the value of C_{max} proportionally. Similarly, a lower E value would allow more deflection at the same σ_{uts}, increasing C_{max} inversely proportionally. Hence the significance of C_{max} depends a lot on the σ/E ratio of a material, with larger ratios increasing its significance. Future work can look into how this ratio varies between anatomical sites, and suggest which versions of this model are most appropriate for which areas. In this paper ANSYS was used to estimate C_{max}. This is difficult to automate and integrate into another system. This can be improved by deriving the underlying 1D differential equation, and solving with simpler generalised techniques (e.g. Finite difference method in MATLAB/python, or analytically if possible).

The mechanics of the initial screw engagement are complex. Future models could work on addressing this, for example by considering linear and angular displacement independently (at least for the engagement phase), rather than assuming they are always proportional.

V. Conclusions

A model was developed to provide a more geometrically generalised model for the self tapping screw insertion process. The results of this model were compared with an existing model from [9], this showed similar but distinct predictions; suggesting the model is reasonable, but may be able to increase modelling accuracy for complex geometries. Overall, this model shows promise in modelling the more geometrically complex aspects of bone screws. Further testing will quantify its accuracy, and/or expose its shortcomings to allow further improvements.

References

[1] M. Evans, M. Spencer, Q. Wang, S. H. White, and J. L. Cunningham, "Design and testing of external fixator bone screws," *Journal of Biomedical Engineering*, vol. 12, no. 6, pp. 457–462, Nov. 1990.

[2] A. Feroz Dinah, S. C. Mears, T. A. Knight, S. P. Soin, J. T. Campbell, and S. M. Belkoff, "Inadvertent Screw Stripping During Ankle Fracture Fixation in Elderly Bone," *Geriatr Orthop Surg Rehabil*, vol. 2, no. 3, pp. 86–89, May 2011.

[3] N. J. Hallab and J. J. Jacobs, "Biologic effects of implant debris," *Bull NYU Hosp Jt Dis*, vol. 67, no. 2, pp. 182–188, 2009.

[4] M. J. Stoesz, P. A. Gustafson, B. V. Patel, J. R. Jastifer, and J. L. Chess, "Surgeon Perception of Cancellous Screw Fixation," *Journal of Orthopaedic Trauma*, vol. 28, no. 1, p. e1, Jan. 2014.

[5] J. Wilkie, P. D. Docherty, and K. Möller, "A simple screwing process model for bone material identification," *Proceedings on Automation in Medical Engineering*, vol. 1, no. 1, pp. 038–038, Feb. 2020.

[6] ——, "Developments in Modelling Bone Screwing," *Current Directions in Biomedical Engineering*, vol. 6, no. 3, pp. 111–114, Sep. 2020.

[7] ——, "Model-based bone material property identification," *at - Automatisierungstechnik*, vol. 68, no. 11, pp. 913–921, Nov. 2020.

[8] J. Wilkie, P. D. Docherty, T. Stieglitz, and K. Möller, "Quantifying Accuracy of Self-Tapping Screw Model," in *2021 43rd Annual IEEE Conference of the IEEE Engineering in Medicine and Biology Society, In Press*, Guadalajara, Mexico, 2021.

[9] L. D. Seneviratne, F. A. Ngemoh, S. W. E. Earles, and K. A. Althoefer, "Theoretical modelling of the self-tapping screw fastening process," *Proceedings of the Institution of Mechanical Engineers, Part C: Journal of Mechanical Engineering Science*, vol. 215, no. 2, pp. 135–154, Feb. 2001.

[10] International Organization for Standardization, "ISO 5835:1991(en), Implants for surgery — Metal bone screws with hexagonal drive connection, spherical under-surface of head, asymmetrical thread — Dimensions," https://www.iso.org/obp/ui/#iso:std:iso:5835:ed-1:v1:en, 1991.

[11] B. Li and R. M. Aspden, "Composition and Mechanical Properties of Cancellous Bone from the Femoral Head of Patients with Osteoporosis or Osteoarthritis," *Journal of Bone and Mineral Research*, vol. 12, no. 4, pp. 641–651, 1997.

[12] A. Shirazi-Adl, M. Dammak, and G. Paiement, "Experimental determination of friction characteristics at the trabecular bone/porous-coated metal interface in cementless implants," *Journal of Biomedical Materials Research*, vol. 27, no. 2, pp. 167–175, 1993.